ACS OMEGA

Open Access

http://pubs.acs.org/journal/acsodf

Article

Crystal Transformation Synthesis of a Three-Dimensional Dual-Fold Building Block Derived from Metal−Organic Framework for Tetracycline Detection

Yang Song,* Yangyang Zhao, Jie Wu, Dongli Deng, Yiqin Duan, Ying Li,* Mingzhu Wu, and Guohua Dong*

Cite This: *ACS Omega* 2025, 10, 3165−3175

Read Online

ACCESS | Metrics & More | Article Recommendations | Supporting Information

ABSTRACT: Metal−organic framework (MOF)-based sensors, which have garnered considerable focus for their potential to enhance environmental monitoring and improve water quality by accurately and consistently identifying antibiotic compounds in water, have gained considerable interest. With the help of pH value, an unusual instance of single-crystal-to-single-crystal (SCSC) transition from the three-dimensional (3D) Zn-framework $\{[Zn_2(mbix)_2(2,5\text{-bda})_2]\cdot H_2O\}_n$ (1) to the 3D 2-fold Zn-framework $\{[Zn_4(mbix)_4(2,5\text{-bda})_4]\cdot H_2O\}_n$ (2) has been observed under mild conditions. This transformation necessitates the replication of structure **1** while simultaneously modifying the angle between the planes of the imidazole and benzene rings. It is noteworthy that the detection capabilities of **2** for tetracyclines (TC) surpass those of other antibiotic analytes in water. Furthermore, the sensing results are in close consistency with the S−V model when TC concentrations fall within the range of 0−0.08 mM. Additionally, the limit of detection (LOD) of the sensor toward TC is estimated to be 0.59 nM. The stronger quenching impact seen for TC can be linked to a more significant overlap in the energy transfer process. The aforementioned proposition presents a viable strategy for the systematic fabrication of economically viable luminescent sensors, thereby enabling efficient and cost-effective modifications of properties.

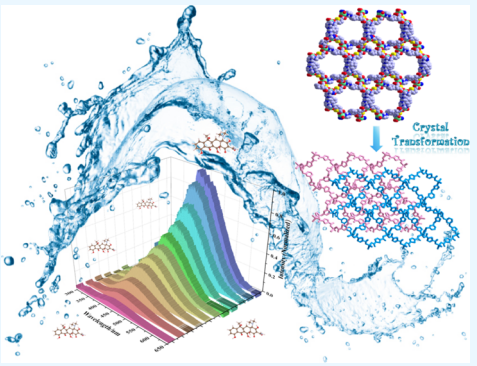

1. INTRODUCTION

Tetracyclines (TC) are a prevalent type of antibiotic utilized in the treatment of infections. However, their overuse has detrimentally impacted both human health and the ecosystem.[1] In the last ten years, various analytical techniques have been described for quantifying TC. Advanced instrumental techniques, such as capillary electrophoresis (CE),[2] liquid chromatography with tandem mass spectrometry (LC−MS),[3] high-performance liquid chromatography (HPLC),[4] and capillary electrophoresis-mass spectrometry (CE-MS)[5] have been employed for the detection of TC. These approaches exhibit superior sensitivity and correctness; however, they are associated with expensive and intricate equipment, complex sample pretreatment procedures,[6] and time-consuming processes,[7] thereby constraining their widespread application.

Fluorescence-based chemical sensors are a field detection technology known for their rapid response time,[8] high sensitivity,[9] and exceptional operability.[10] Metal−organic frameworks (MOFs)[11,12] have recently attracted interest as a potential medium for the detection of trace contaminants in water.[13−15] This is primarily owed to their high surface-to-volume ratio, exceptional porosity, and adaptable structure and functionalities. Specifically, fluorescent MOFs have shown the ability to rapidly, conveniently, and visually detect organic pollutants and antibiotics by leveraging their high-purity fluorescence color[16,17] and long excited-state lifetime.[18] In spite of the widespread use of fluorescent MOF materials as promising chemical sensors,[19,20] only a few have shown the capability to detect antibiotics in an aqueous phase.[21,22] This presents challenges from both experimental and practical perspectives in antibiotic detection in wastewater using fluorescence-based chemical sensor materials.[23]

The occurrence of reactions occurring in the single-crystal-to-single-crystal (SCSC) is rare due to the inherent challenge of maintaining the structural integrity of the crystal while accommodating atomic movement.[24,25] However, the SCSC transformation remains highly advantageous as it facilitates the creation of novel MOF types with high yields, which are otherwise unachievable under traditional conditions.[26] The research on SCSC conversion primarily focuses on the

Received: November 21, 2024
Revised: December 26, 2024
Accepted: January 6, 2025
Published: January 11, 2025

desorption or adsorption of the target molecule within the MOFs. We believe that Zinc(Zn) is an ideal candidate for constructing MOFs[27−29] because it has a larger ion size, broader coordination characteristics, and lower toxicity within the constituents, which can form MOFs with various structures, sufficient electron, and luminescent properties.[30−32] The compound 2,5-thiophenedicarboxylic acid (2,5-H_2tdad), characterized by the 120° bond angle between the thiophene ring and its two carboxylate groups, serves as a flexible ligand. This flexibility stems from its capacity to function as a bidentate or tridentate ligand, a feature that it owes to the strategic placement of its functional groups. The compound 1,3-bis(imidazol-1-ylmethyl)benzene (m-bix), possessing two adaptable $-CH_2-$ units, can offer diverse coordination modes. These modes enable the formation of both isolated and extended coordination compounds under appropriate synthetic conditions.[33] The aforementioned phenomenon was utilized to apply KOH with a pH-driven SCSC transformation strategy. This application successfully converted 3D metal−organic framework (MOF) $\{[Zn_2(mbix)_2(2,5\text{-}bda)_2]\cdot H_2O\}_n$ (**1**) into another 3D MOF $\{[Zn_4(mbix)_4(2,5\text{-}bda)_4]\cdot H_2O\}_n$ (**2**). This conversion was achieved by replicating the structure of MOF 1 and elongating the Zn−N bonds.

2. EXPERIMENTAL PART

2.1. Synthesis of $\{[Zn_2(mbix)_2(2,5\text{-}bda)_2]\cdot H_2O\}_n$ (1). $Zn(NO_3)_2\cdot 6H_2O$ (0.030 g), m-bix (0.024 g), and 2,5-H_2tdad (0.017 mg) in a 1:1:1 molar ratio was dissolved in 5 mL of H_2O. The solution was then transferred to a 20 mL Teflon-lined stainless steel vessel and subjected to autogenous pressure, followed by heating at 160 °C for 120 h. After it was gradually cooled to room temperature, the mixture was rinsed with distilled water. The resulting light yellow, transparent, and block-shaped crystals were filtered and allowed to dry at 25 °C (yielding approximately 57% based on m-bix). Elemental analysis (%): Calculated for $C_{40}H_{34}N_8O_9S_2Zn_2$ (Mr: 965.65): C, 49.75; N, 11.60; H, 3.55% Found: C, 49.73; N, 11.59; H, 3.56%. FT-IR (KBr, cm^{-1}): 3428(br, s), 3123(m), 1559(s), 1524(s), 1433(w), 1382(s), 1284(w), 1225(m), 1147(w), 1091(m), 1017(m), 939(m), 816(m), 776(s), 646(m), 528(w).

2.2. Synthesis of $\{[Zn_4(mbix)_4(2,5\text{-}bda)_4]\cdot H_2O\}_n$ (2). Crystals of **1** were soaked in 0.1 mol/L KOH, and the pH was adjusted to 8.5. The solution was then moved to a 20 mL Teflon-lined stainless steel vessel and heated at 160 °C for 48 h. After gradually cooling to 25 °C, pale yellow crystals were obtained (yielding 48% based on m-bix). Elemental analysis (%): Calculated for $C_{80}H_{66}N_{16}O_{17}S_4Zn_4$ (Mr: 1913.29): C, 50.22%; N, 11.71%; H, 3.48%. Found: C, 50.24%; N, 11.72%; H, 3.47%. FT-IR (KBr, cm^{-1}): 3422(br, s), 3129(m), 1553(s), 1524(s), 1445(w), 1375(s), 1238(m), 1153(w), 1091(m), 1030(m), 939(m), 822(m), 783(s), 659(m), 522(w).

2.3. X-Ray Crystal Structure Determination. The crystallographic data for **1** and **2** can be found in CCDC 1436801 and 1436802, respectively, and are available free of charge at www.ccdc.cam.ac.uk/deposit. Table 1 provides the crystal structure data along with the details of data collection and structure refinement. Table S1 lists the selected bond lengths and bond angles for the MOFs.

Table 1. Crystal Data and Structure Refinement Parameters of MOFs 1 and 2[a,b]

identification code	1	2
empirical formula	$C_{40}H_{34}N_8O_9S_2Zn_2$	$C_{80}H_{66}N_{16}O_{17}S_4Zn_4$
formula mass	965.65	1913.29
crystal system	monoclinic	monoclinic
space group	P_c	P_n
a (Å)	11.8021(8)	8.7833(15)
b (Å)	11.3518(17)	28.682(5)
c (Å)	15.9416(12)	16.212(3)
α (deg)	90	90
β (deg)	105.844(2)	95.675(11)
γ (deg)	90	90
V (Å^3)	2054.6(2)	4064.2(12)
Z	2	2
D_c (g·cm^{-3})	1.561	1.563
μ (Mo Kα) (mm^{-1})	1.335	1.348
F(000)	988	1956
2θ range (deg)	3.083−24.997	1.448−25.368
limiting indices	$-14 \le h \le 14$	$-10 \le h \le 10$
	$-13 \le k \le 13$	$-34 \le k \le 34$
	$-18 \le l \le 16$	$-19 \le l \le 18$
data/restraints/parameters	6299/2/550	13124/9/1091
GOF on F^2	1.046	1.077
final R indices [$I > 2\sigma(I)$]		
R_1	0.0436	0.079
wR_2	0.0875	0.1318
R indices (all data)		
R_1	0.0673	0.1394
wR_2	0.0969	0.1581
CCDC	1436801	1436802

[a] $R_1 = \sum||F_0| - |F_c||/\sum|F_0|$. [b] $wR_2 = [\sum[w(F_0^2 - F_c^2)^2]/\sum[w(F_0^2)^2]]^{1/2}$.

3. RESULTS AND DISCUSSION

3.1. Syntheses and Crystal Structure. The three-dimensional metal−organic framework **1** was synthesized via hydrothermal methods and subsequently utilized as a precursor to generate the novel three-dimensional MOF $\{[Zn_4(mbix)_4(2,5\text{-}bda)_4]\cdot H_2O\}_n$(**2**). This process demonstrates a seldom-observed 3D → 3D structural transformation, which replicates structure **1** and modifies the angle between the planes of the imidazole ring and benzene ring. This is accomplished by manipulating the pH value of the reaction mixture that was measured. The chemical formulas of MOFs **1** and **2** are the same. MOF **1** crystallizes in the monoclinic P_c space group, as illustrated in Figure 1a; the fundamental structural unit of **1** comprises two independent Zn^{2+} ions, two coordinated m-bix ligands, two coordinated 2,5-tdad^{2-} anions, and one uncoordinated water molecule. In MOF **1**, the organic carboxylic acid ligand 2,5-H_2tdad is fully deprotonated and thus involved in coordination with the central metal. The dihedral angles between the two imidazole rings and the phenyl ring of the m-bix ligand, when coordinated with Zn^{2+}, measure 65.00 and 80.16°, respectively. Conversely, the angles of rotation between the two imidazole rings are determined to be 75.41 and 72.04°, respectively (Figure 1c). The flexible $-CH_2-$ moiety allows each m-bix ligand to exhibit varying twisting angles when connecting two metal ions, and three metal ions form a ternary ring secondary structure by linking two 2,5-tdad^{2-} anions and one m-bix ligand. Additionally, eight metal ions connect four 2,5-tdad^{2-} anions and four m-bix

https://doi.org/10.1021/acsomega.4c10594
ACS Omega 2025, 10, 3165−3175

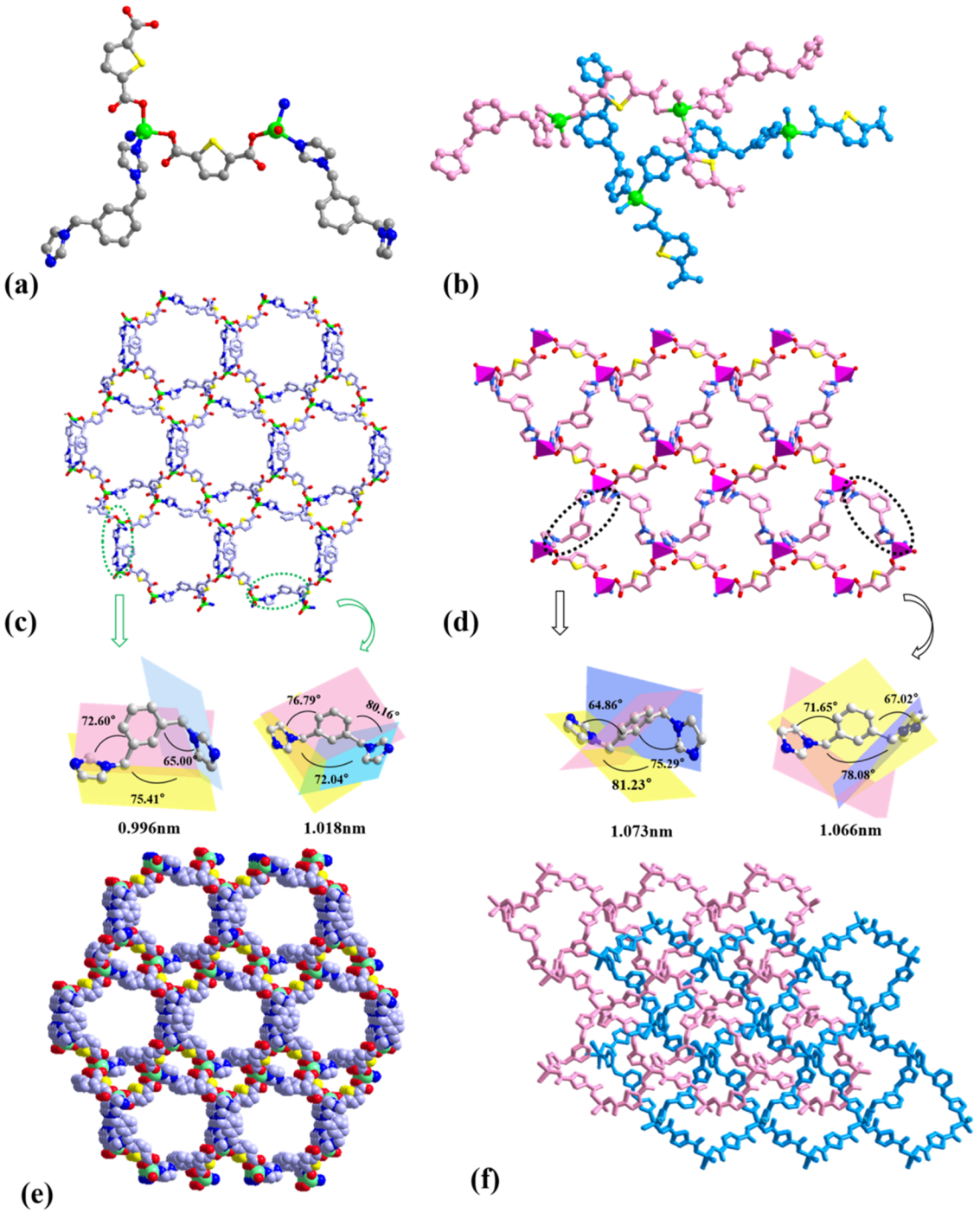

Figure 1. (a) Coordination environment surrounding the Zn^{II} metal ions in **1**; (b) coordination environment around the Zn^{II} metal ions in **2**; (c) two-dimensional framework of **1**; (d) two-dimensional layer of **2** viewed in the ac plane; (e) three-dimensional framework of MOF **1**; and (f) three-dimensional framework of MOF **2**.

ligands to form an octahedral ring secondary structure. The interlacing connection of these ternary ring secondary structures with octahedral ring secondary structures results in a two-dimensional pore structure for **1**, and adjacent two-dimensional pore structures alternate and connect to create a three-dimensional network structure (Figure 1e). If each Zn^{2+} metal ion is considered a four-connected node linked to both the m-bix ligand and 2,5-tdad^{2-} anion (considered connecting lines), to better understand, we can simplify the crystal structure of **1** as a (4,4) network topology with connectivity, as illustrated in Figure S1.

Given the aforementioned bonding environment, it is plausible that suitable conditions exist for the twisting of the angle between the planes of the benzene rings and imidazole rings. The addition of KOH, which consequently elevated the pH values of the reaction spanning from 4.5 to 8.5, precipitated changes within the crystal structure. The elevated pH and sustained high temperature, accompanied by conformational transformation from 3D MOF **1** to 3D compact interweaving MOF **2**, are illustrated in the reaction routes of MOFs **1** and **2**, as shown in Scheme 1.

https://doi.org/10.1021/acsomega.4c10594
ACS Omega 2025, 10, 3165−3175

Scheme 1. Reaction Materials and Routes of 1 and 2

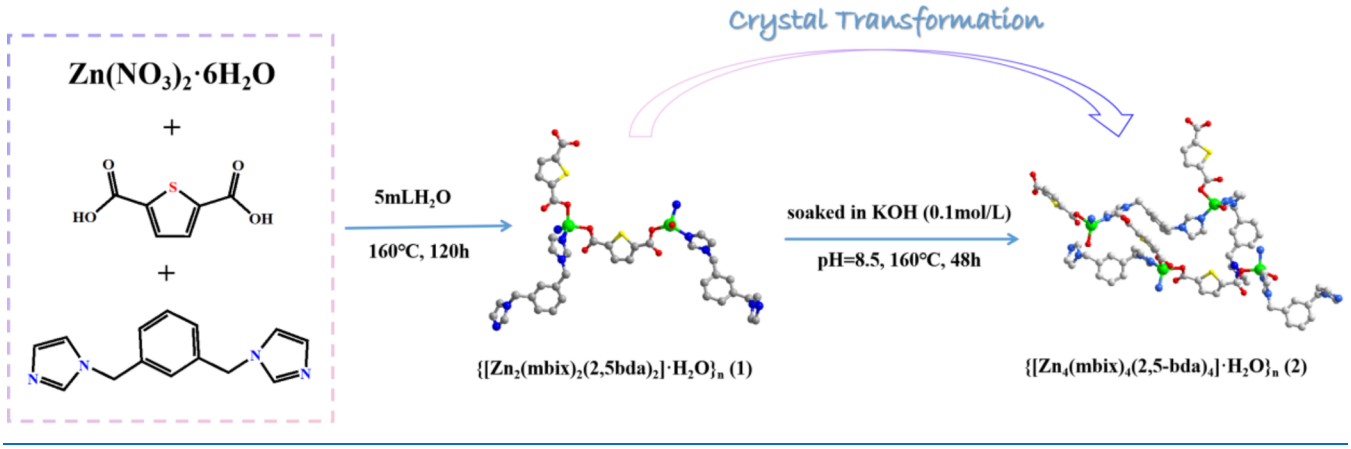

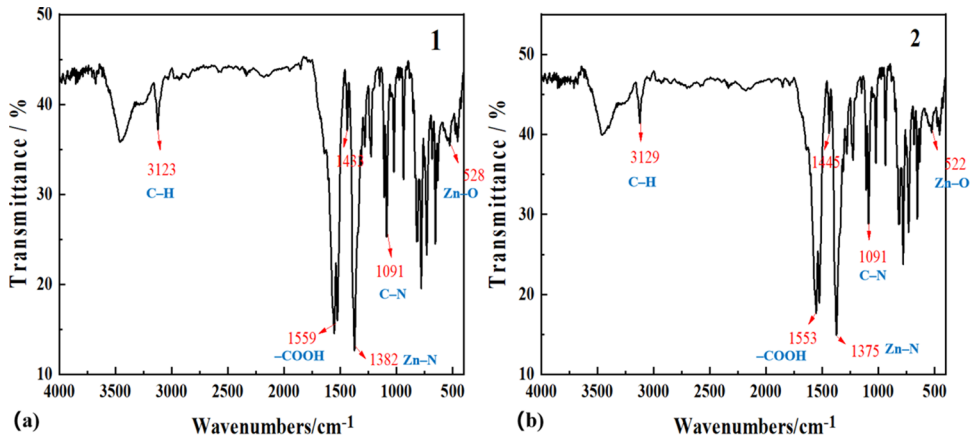

Figure 2. IR spectra of 1 (a) and 2 (b).

In contrast to the P_c space group of 1, MOF 2 adopts the monoclinic space group P_n. The structure of 2 is composed of two identical fundamental structural units, which are also present in 1 (Figure 1b). In both structures (1 and 2), the Zn^{2+} ions adopt a tetragonal coordination environment where they coordinate with the m-bix ligand, which contains two nitrogen atoms, and the 2,5-tdad^{2-} anion, which contains two oxygen atoms. This coordination environment exhibits a slightly twisted trigonal cone geometry [ZnN_2O_2]. The Zn−O bond lengths vary from 1.920(6) to 1.987(6) Å, while those between Zn and N range from 1.983(6) to 2.036(7) Å. These bond lengths are consistent with previously reported values.[34,35] Each fundamental structural unit can be expanded into a 3D porous network structure. The presence of pores allows the two fundamental structural units in 2 to intertwine, forming a compact structure. This intricate interweaving of the basic structural units ultimately results in the unique 3D → 3D structure of 2 (Figure 1f). Superimposing the structure of 2 leads to the formation of a compact framework exhibiting interpenetration.

Upon comparison of the structures of MOFs 1 and 2, it is evident that the primary ligand serving a connective role is the ligand of m-bix. The existence of the flexible −CH_2− group results in the alterations to the dihedral angles of the m-bix. The angle between the planes of the benzene and imidazole rings in one of the m-bix has changed from 72.60 to 64.86° and the other one from 65.00 to 75.29°, which causes the m-bix to extend. The ligand length has increased from 0.996 to 1.073 nm. In the other m-bix, the dihedral angles between the benzene ring and the imidazole ring changed from 76.79 to 71.65° and from 80.16 to 67.02° (Figure 1d). Both dihedral angles are in a state of contraction. As previously mentioned, alterations in the dihedral angles and ligand lengths have resulted in changes in the pores within the 2D structures of the two metal−organic frameworks (MOFs).

3.2. IR Spectroscopy. The infrared spectra for MOFs 1 and 2 have been captured within the wavelength range of 4000−400 cm^{-1}, as illustrated in Figure 2. Given that the compositions of 1 and 2 are identical, their IR spectra display analogous peak positions, albeit with varying intensities. The absorption bands at around 3123 and 3129 cm^{-1} can be assigned to the C−H stretching vibrations of the benzene ring within the functional group region. The absorption peaks corresponding to the asymmetric and symmetric stretching vibrations of the carboxyl functional group appear around 1559 and 1433 cm^{-1}, as well as at 1553 and 1445 cm^{-1}, respectively. The absorption bands observed near 1382 and 1375 cm^{-1} are attributed to the Zn−N coordination bond. Additionally, the absorption signal at approximately 1091 cm^{-1} in the IR spectrum is associated with C−N stretching vibrations. Weak absorption bands at 528 and 522 cm^{-1} are assigned to the stretching vibrations of the Zn−O bond.[36]

3.3. Powder X-ray Diffraction (PXRD) and Thermal Analysis. To confirm the phase purity of MOFs 1 and 2, their powder X-ray diffraction (PXRD) patterns were measured at 25 °C. A significant agreement was observed between the

https://doi.org/10.1021/acsomega.4c10594
ACS Omega 2025, 10, 3165−3175

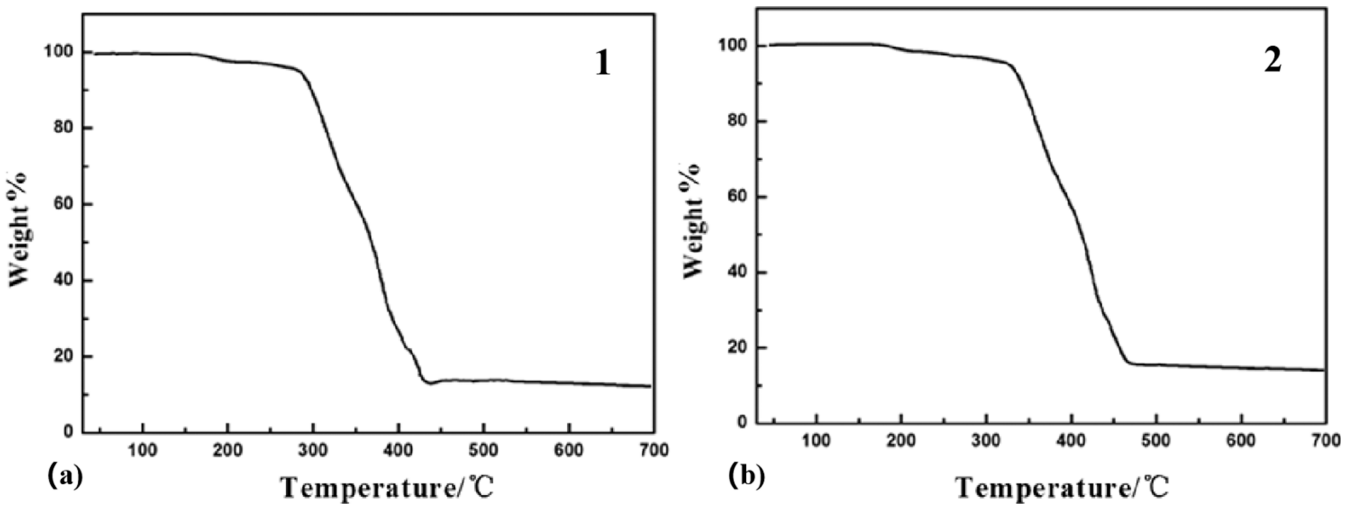

Figure 3. TG curves of **1** (a) and **2** (b).

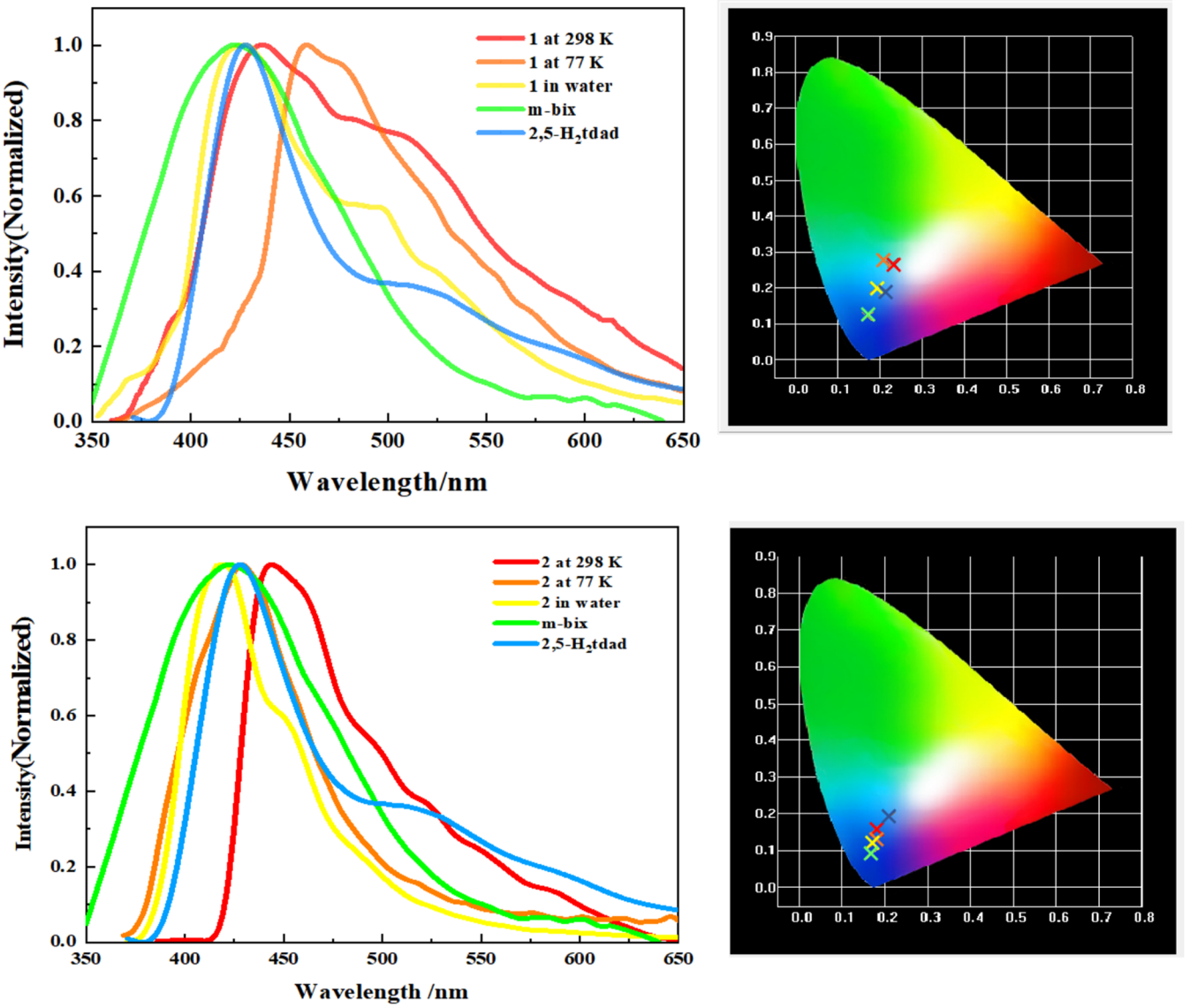

Figure 4. Emission spectra of MOFs **1** and **2** were recorded in the solid state at temperatures of 298 K (delineated by the red line) and 77 K (represented by the orange line) as well as in a water medium (outlined by the yellow line). The emission spectra of m-bix (highlighted by the green line) and 2,5-H_2tdad (denoted by the blue line) and the relevant color coordinate chart of the emissions.

https://doi.org/10.1021/acsomega.4c10594
ACS Omega 2025, 10, 3165−3175

Table 2. Luminescent Data for 1−2 at 298 and 77 K in the Solid State and in Water and Luminescent Data for Ligands at 298 K

compound	temperature (K)	excitation (λ_{ex}, nm)	emission (λ_{em}, nm)	CIE 1931 (x, y)	τ_1 (μs)	τ_2 (μs)	$<\tau>$ (μs)
1	298	330	436	(0.23, 0.27)	1.11 (73.71%)	8.95 (26.29%)	6.93
	77	330	459	(0.21, 0.28)	0.94 (61.17%)	8.31 (38.83%)	7.20
	water	330	427	(0.19, 0.20)	1.17 (63.57%)	8.11 (36.43%)	6.71
2	298	330	427	(0.18, 0.16)	0.81 (80.11%)	7.50 (19.89%)	5.47
	77	330	446	(0.18, 0.13)	0.93 (80.31%)	8.11 (19.69%)	5.82
	water	330	419	(0.17, 0.09)	0.85 (87.42%)	7.89 (12.58%)	4.88
m-bix	298	330	422	(0.17, 0.12)	1.46 (62.91%)	8.06 (37.09%)	6.51
2,5-H_2tdad	298	330	425	(0.21, 0.19)	0.85 (24.92%)	6.30 (75.08%)	6.07

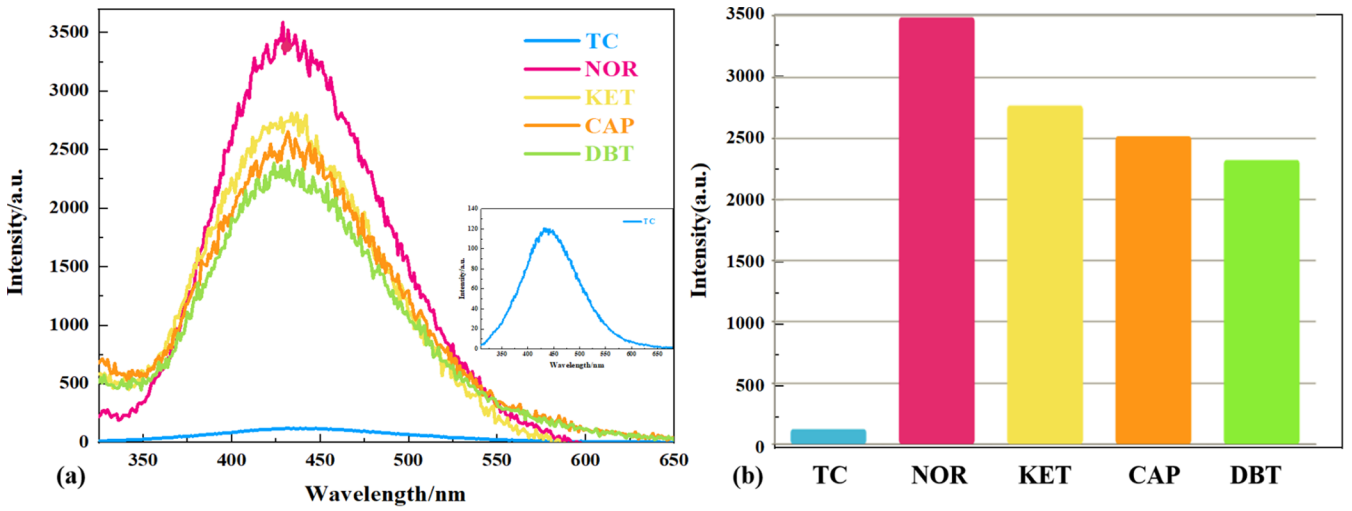

Figure 5. (a) Emission spectrum of **2** in different antibiotics; inset: emission spectra of **2** in TC. (b) Luminescence intensity bar chart of **2** in various organic solvents.

experimental and simulated PXRD patterns for both MOFs (Figure S2).

The stability of the MOFs was estimated by using thermogravimetric analyses (TGA). Figure 3 displays the corresponding TGA curves. In the thermogravimetric curve of MOF **1**, the initial stage exhibits a weight loss temperature range from 153 to 204 °C, which is associated with the release of one water molecule in the crystal structure (found: 1.88%, calculated: 1.87%). Evidently, the structure of **1** remains intact until 434 °C. Similarly, **2** also undergoes dual-stage weight loss: its primary stage occurs within a temperature interval between 176 and 205 °C, resulting in a weight loss rate of 1.02% linked to the loss of one free H_2O in the crystal structure (calculated 0.94%). Subsequently, the loss of 84.37% that occurs at the depletion of ligands accounts for the second step within the temperature range of 293−457 °C, which accounts for a calculated 85.81%. In comparison with **1**, MOF **2** exhibits a compact structure comprising interpenetrating double layers. The crystal framework remains stable up to 457 °C, rivaling the best among these MOFs.[37,38]

3.4. Luminescence Property. Metal−organic frameworks, comprising both metal and organic ligands, particularly those with d^{10} electron configurations, have the potential to function as photosensitive materials.[39] Consequently, it is immensely beneficial to investigate the fluorescence characteristics of **1** and **2** in their solid state at both 298 and 77 K, as well as in water, to elucidate the correlation between the structure and emission (Figure 4 and Table 2). The emission spectra in the solid state of two Zn-containing MOFs at 298 K are centered at 436 and 427 nm, respectively, producing blue luminescence with Commission Internationale d'Eclairage (CIE) coordinates of (0.23, 0.27) for MOF **1** and (0.18, 0.16) for MOF **2**. The emission originating from the ligands implies an energy transfer occurring from one ligand to another during the process of photoluminescence. Therefore, the emissions may be assigned to a LLCT.[40] This particular phenomenon has been previously noted in a series of Zn(II) MOFs, which were supported by N-donor bridges and incorporated varying coligands.

The emission spectra of both MOFs exhibit a marked narrowing in the solid state at 77 K, compared to those recorded at 298 K. Specifically, **1** and **2** exhibit a pronounced red-shifted chromic process, with transitions from 436 → 459 and 427 → 446 nm, respectively. MOF **1** emits strong green luminescence with CIE coordinates of (0.34, 0.59), while MOF **2** generates light green luminescence with CIE coordinates of (0.18, 0.13), positioning it within the blue wavelength range. This observed phenomenon is referred to as "luminescence thermochromism"[41] and has also been documented in prior literature.[42] For both MOFs **1** and **2**, the maximum emission peak of MOF **2** is blue-shifted compared to that of MOF **1**, a difference likely caused by the more compact structure of MOF **2**, which hinders electron transmission. The luminescence lifetimes of **1**−**2** are shown in Figure S3.

3.5. Detection of Tetracyclines. Next, MOF **2** was employed as a chemical sensor for detecting antibiotics in water. A powdered sample (5 mg) was suspended in 3 mL of

https://doi.org/10.1021/acsomega.4c10594
ACS Omega 2025, 10, 3165−3175

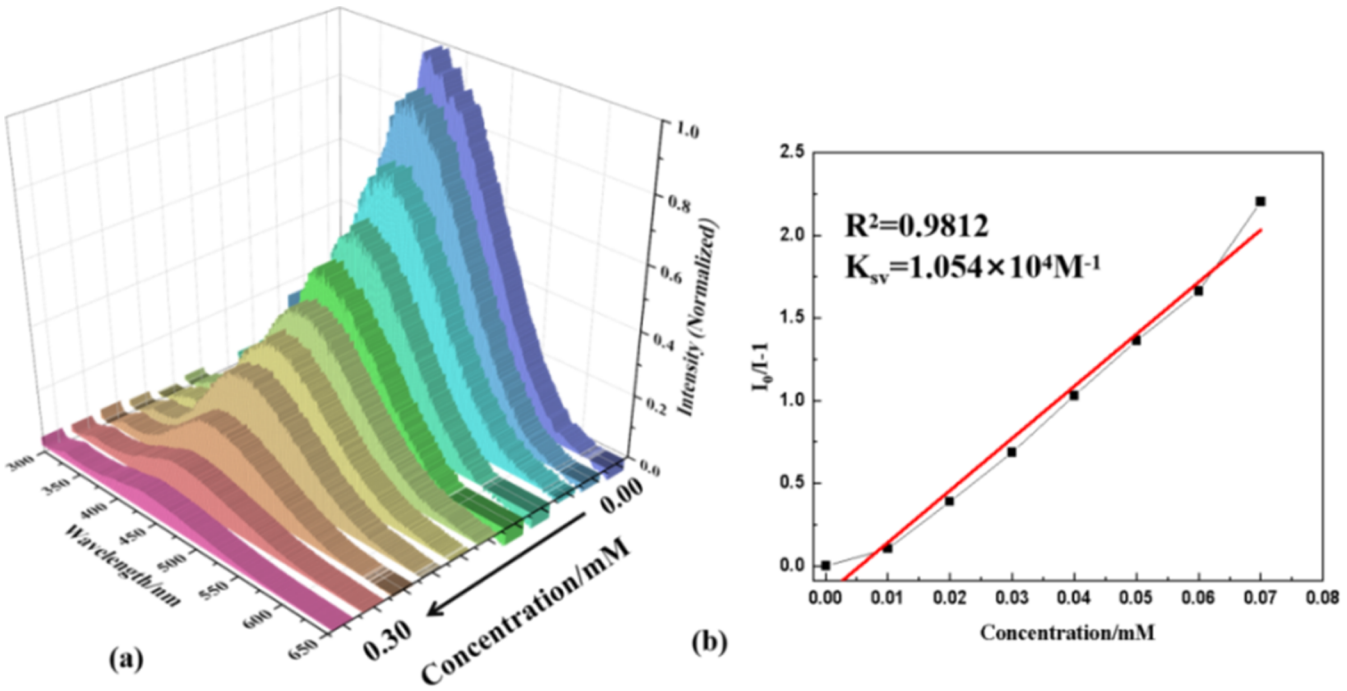

Figure 6. (a) Fluorescence intensity of **2** in different concentrations at ca. 427 nm (λ_{ex} = 330 nm); (b) linear relationship of **2** quenched in different concentrations of TC.

aqueous antibiotic solutions at a concentration of 1×10^{-4} M prior to the measurement of the emission spectra. As expected, **2** exhibited detectable fluorescence-quenching effects on five chosen antibiotics in aqueous solutions, including tetracyclines (TC), norfloxacin (NOR), ketoprofen (KET), chloramphenicol (CAP), and dibenzothiophene (DBT). The most notable feature is the significant dependence of the photoluminescent spectra on the antibiotic compounds, particularly in the case of TC, which shows the most significant quenching phenomena (Figure 5). These promising results suggest that MOF **2** could serve as an effective luminescent probe for detecting small tetracycline molecules.

To gain a deeper understanding of the response exhibited by **2** toward TC, an investigation was conducted into the relationship between luminescence and TC concentration. The comprehensive experimental methodology is delineated in the Supporting Information. In Figure 6a, there was a gradual decrease in the luminescence of the **2** suspension as the TC concentration increased. Simultaneously, under UV lamp irradiation, the appearance of the suspension changed from blue to colorless. The quantitative representation of the linear relationship between luminescence and TC concentration can be effectively articulated through the Stern−Volmer (S−V) formula[43]

$$I_0/I = K_{SV}[C] + 1$$

I_0 and I represent the luminescence intensities of the suspension before and after mixing with TC, respectively. $[C]$ represents the molar concentration of the TC solutions, while K_{SV} is the Stern−Volmer quenching constant (M^{-1}).

The S−V plots in Figure 6b demonstrate a linear correlation coefficient (R^2) of 0.9812 for TC, indicating that the sensing results align well with the S−V model when TC concentrations are within the range of 0−0.08 mM. The K_{SV} value for TC is calculated to be 1.05×10^4 M^{-1}. Additionally, the limit of detection (LOD) of the sensor toward TC is estimated to be 0.59 nM, based on the 3σ IUPAC criteria.[44] Compared to previously reported results (Table 3), the LOD for tetracycline (TC) is on par with the sophisticated, high-performance liquid chromatography (HPLC)[45] and carbon electrode[46] methods, and it also surpasses the sensitivity of several other chemosensors.[47] Consequently, this study introduces another highly sensitive chemosensor for real-time monitoring of TC.

Table 3. Comparisons of LOD and the Linearity Range in the Detection of TC

LOD	linear range	method	ref
1.1 nM		HPLC	45
0.6 nM	1×10^{-6} to 5×10^{-3} M	carbon electrode	46
0.017 nM		electrochemical multiplex immunoassay	47
22.4 nM/L		MSPE	48
237/224 nM		microbiological assay	49
0.10 μM		ECL	50
1.4 nM	0.10−6.0 mg/L	silver nanoparticles	51
0.14 μM	0−15 μM in milk	CdTe quantum dots	52
0.59 nM	0−0.08 mM	fluorescent probe	this work

3.6. Mechanism of Detecting Tetracyclines. Explanations based on the mechanisms of electron transfer[53,54] and resonance energy transfer[55,56] have been extensively validated for elucidating the phenomenon of fluorescence attenuation in **2** and its exceptional capability for TC detection. From an electron transfer perspective, the energy level of the conduction band[57] in the electron-rich MOF **2** is generally higher than the lowest unoccupied molecular orbital (LUMO) of the analyte. Upon ultraviolet excitation, excited electrons transfer from the conduction band of the MOF to the LUMOs of the analyte. Moreover, as a driving force, the quenching effect on fluorescence becomes more pronounced with an

https://doi.org/10.1021/acsomega.4c10594
ACS Omega 2025, 10, 3165−3175

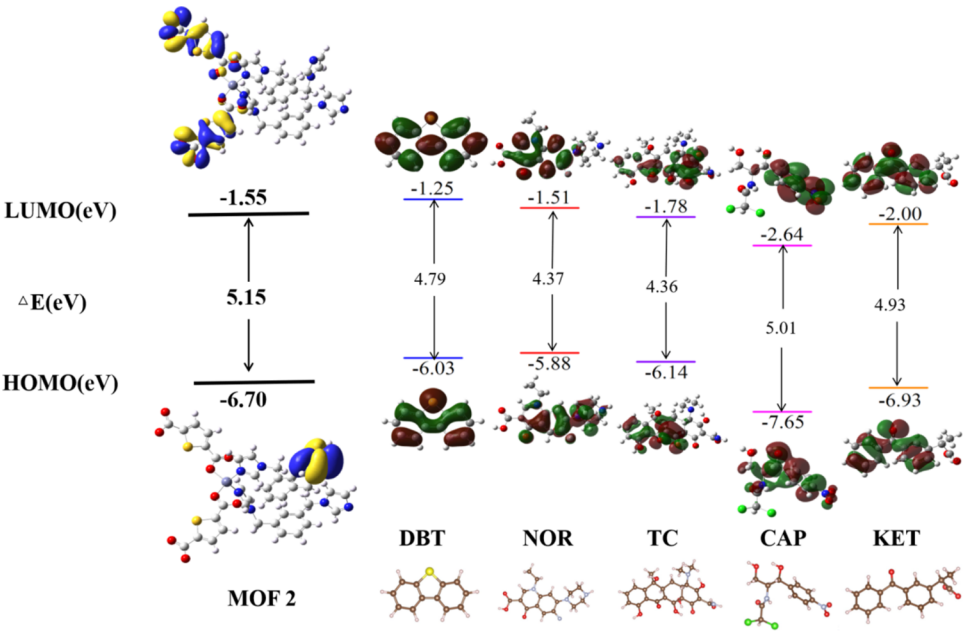

Figure 7. Schematic representation of the potential electron transfer pathway from **2** to antibiotic analytes.

increasing energy difference. As shown in Figure 7, the remarkable efficiency exhibited by **2** in terms of fluorescence quenching aligns well with the low LUMO energy observed in various tested analytes.

To account for the difference between the observed quenching efficiency and the calculated LUMO level, the resonance energy transfer mechanism is employed; the energy transfer process is widely recognized as occurring when fluorescence emission overlaps with ultraviolet absorption. The efficiency of this transfer is determined by the degree of this overlap. Consequently, ultraviolet−visible spectra of the analytes were recorded. The results, shown in Figure 8, indicate a significant overlap between the absorption band of TC and the emission band of **2**, while minimal or no overlap is observed for the other analytes. This explains the highly efficient quenching performance of **2** toward TC.

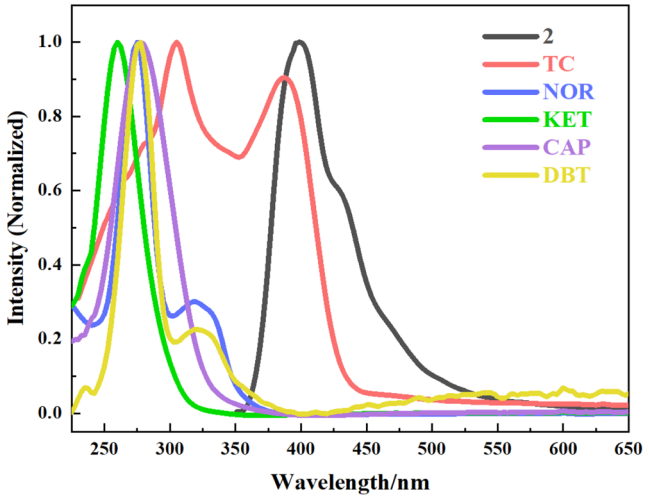

Figure 8. Spectral overlaps between the normalized absorption spectra of selected antibiotics and the normalized emission spectrum of **2** in water.

The results further underscore the predominance of energy transfer between these two mechanisms, which is consistent with their distinct quenching responses to TC. The electron transfer process remains similar due to the proximity of LUMO energy levels. However, the more pronounced quenching effect noted in TC can be ascribed to a greater degree of overlap in the energy transfer process.

4. CONCLUSIONS

In a word, we have presented an original three-dimensional MOF **1** with a (4,4) connected network topology that undergoes structural transformation to form another three-dimensional MOF **2** upon SCSC transformation. The transformation process involves replicating the structure of **1** and modulating the pH value. This alters the dihedral angle between the imidazole and benzene rings, a phenomenon that is infrequently observed in MOFs. The SCSC behavior observed in **1** can be attributed to host−guest interactions and its intrinsic features, such as ligand flexibility allowing for deformation. Furthermore, **2** exhibits excellent detection ability toward TC compared to other antibiotic analytes. The electron transfer process remains similar due to the close proximity of LUMO energy levels; however, the stronger quenching effect observed for TC can be attributed to a greater degree of overlap in the energy transfer process. Overall, our research results provide valuable insights into achieving 2-fold interpenetration in a three-dimensional structure through a SCSC transformation.

■ ASSOCIATED CONTENT

Supporting Information

The Supporting Information is available free of charge at https://pubs.acs.org/doi/10.1021/acsomega.4c10594.

The table of selected bond lengths and angles; regents and materials; experimental details; the figure of (4,4) connected network topology of **1**; the PXRD patterns; and the decay curves and emission spectra (PDF)

Crystallographic data (CIF)

https://doi.org/10.1021/acsomega.4c10594
ACS Omega 2025, 10, 3165−3175

AUTHOR INFORMATION

Corresponding Authors

Yang Song − *Chemical Pollution Control Chongqing Applied Technology Extension Center of Higher Vocational Colleges, Chongqing Industry Polytechnic College, Chongqing 401120, P. R. China;* orcid.org/0009-0006-7928-115X; Email: songyang@cqipc.edu.cn; Fax: +86-023-61879390

Ying Li − *Chemical Pollution Control Chongqing Applied Technology Extension Center of Higher Vocational Colleges, Chongqing Industry Polytechnic College, Chongqing 401120, P. R. China;* orcid.org/0000-0002-7043-9962; Email: yingli@cqipc.edu.cn

Guohua Dong − *College of Chemistry and Chemical Engineering, Qiqihar University, Qiqihar 161006, P. R. China;* orcid.org/0000-0001-5972-5418; Email: ghdong@qqhru.edu.cn

Authors

Yangyang Zhao − *Chemical Pollution Control Chongqing Applied Technology Extension Center of Higher Vocational Colleges, Chongqing Industry Polytechnic College, Chongqing 401120, P. R. China*

Jie Wu − *Chemical Pollution Control Chongqing Applied Technology Extension Center of Higher Vocational Colleges, Chongqing Industry Polytechnic College, Chongqing 401120, P. R. China*

Dongli Deng − *Chemical Pollution Control Chongqing Applied Technology Extension Center of Higher Vocational Colleges, Chongqing Industry Polytechnic College, Chongqing 401120, P. R. China;* orcid.org/0009-0004-8248-9758

Yiqin Duan − *Chemical Pollution Control Chongqing Applied Technology Extension Center of Higher Vocational Colleges, Chongqing Industry Polytechnic College, Chongqing 401120, P. R. China*

Mingzhu Wu − *Chemical Pollution Control Chongqing Applied Technology Extension Center of Higher Vocational Colleges, Chongqing Industry Polytechnic College, Chongqing 401120, P. R. China*

Complete contact information is available at: https://pubs.acs.org/10.1021/acsomega.4c10594

Notes

The authors declare no competing financial interest.

ACKNOWLEDGMENTS

This work was supported by the Science and Technology Research Program of Chongqing Municipal Education Commission (Grant No. KJQN202303216 and KJZD-K202403201), the Natural Science Foundation of Chongqing (No. CSTB2024 NSCQ-MSX0004), the Chongqing Postdoctoral Science Fund (No. CSTB2023NSCQ-BHX0035), and the Doctoral Fund of Chongqing Industry Polytechnic College (No.2024GZYBSK1-04).

REFERENCES

(1) Li, C. P.; Long, W. W.; Lei, Z.; Guo, L.; Xie, M. J.; Lü, J.; Zhu, X. D. Anionic Metal-Organic Framework as a Unique Turn-on Fluorescent Chemical Sensor for Ultra-Sensitive Detection of Antibiotics. *Chem. Commun.* **2020**, *56*, 12403−12406.

(2) Moreno-González, D.; Lara, F. J.; Jurgovska, N.; Gamiz-Gracia, L.; GarcíaCampana, A. M. Determination of Aminoglycosides in Honey by Capillary Electrophoresis Tandem Mass Spectrometry and Extraction with Molecularly Imprinted Polymers. *Anal. Chim. Acta* **2015**, *891*, 321.

(3) Blasco, C.; Corcia, D. A.; Pico, Y. Determination of Tetracyclines in Multi-Specie Animal Tissues by Pressurized Liquid Extraction and Liquid Chromatography-Tandem Mass Spectrometry. *Food Chem.* **2009**, *116*, 1005.

(4) Liu, H.; Gan, N.; Chen, Y.; Li, T.; Cao, Y. Three Dimensional M × N Type Aptamerfunctionalized Solid-Phase Micro Extraction Fibers Array for Selectively Sorptive Extraction of Multiple Antibiotic Residues in Milk. *RSC Adv.* **2017**, *7*, 6800−6808.

(5) Tong, J.; Rao, Q.; Zhu, K.; Jiang, Z.; Ding, S. Simultaneous Determination of Five Tetracycline and Macrolide Antibiotics in Feeds Using HPEC. *J. Sep. Sci.* **2009**, *32*, 4254−4260.

(6) Tabrizchi, M.; ILbeigi, V. Detection of Explosives by Positive Corona Discharge Ion Mobility Spectrometry. *J. Hazard. Mater.* **2010**, *176*, 692−696.

(7) Blasco, C.; Corcia, A. D.; Pico, Y. Determination of Tetracyclines in Multi-Specie Animal Tissues by Pressurized Liquid Extraction and Liquid Chromatography-Tandem Mass Spectrometry. *Food Chem.* **2009**, *116*, 1005−1012.

(8) Zhu, X. D.; Zhang, K.; Wang, Y.; Long, W. W.; Sa, R. J.; Liu, T. F.; Lv, J. Fluorescent Metal−Organic Framework (MOF) as a Highly Sensitive and Quickly Responsive Chemical Sensor for the Detection of Antibiotics in Simulated Wastewater. *Inorg. Chem.* **2018**, *57*, 1060−1065.

(9) Xing, K.; Fan, R. Q.; Wang, J. Q.; Zhang, S. Q.; Feng, K.; Du, X.; Song, Y.; Wang, P.; Yang, Y. L. Highly Stable and Regenerative Metal−Organic Framework Designed by Multiwalled Divider Installation Strategy for Detection of Co(II) Ions and Organic Aromatics in Water. *ACS Appl. Mater. Interfaces* **2017**, *9*, 19881−19893.

(10) Li, X. Y.; Wang, Z.; Su, H. F.; Feng, S.; Kurmoo, M.; Tung, C. H.; Sun, D.; Zheng, L. S. Anion-Templated Nanosized Silver Clusters Protected by Mixed Thiolate and Diphosphine. *Nanoscale* **2017**, *9*, 3601−3608.

(11) Guo, X. Z.; Lin, B.; Xiong, G. Z.; Krishna, R.; Zhang, Z. R.; Liu, Q. Z.; Zhang, Z. X.; Fan, L. M.; Zhang, J.; Li, B. W. Construction of Negative Electrostatic Sugared Gourd Pore within Nickel-Based Metal-Organic Framework for One-Step Purification Acetylene from Ethylene and Carbon Dioxide Mixture. *Chem. Eng. J.* **2024**, *498*, No. 154734.

(12) Zhao, D. S.; Li, W. Q.; Wen, R. M.; Li, W. C.; Liu, X.; Zhang, X. T.; Fan, L. M. Tb(III) Functionalized MOF Based Self-Calibrating Sensor Integrated with Logic Gate Operation for Efficient Epinephrine Detection in Serum. *J. Rare Earths* **2024**, *42*, 987.

(13) Kreno, L. E.; Leong, K.; Farha, O. K.; Allendorf, M.; Van Duyne, R. P.; Hupp, J. T. Metal−Organic Framework Materials as Chemical Sensors. *Chem. Rev.* **2012**, *112*, 1105−1125.

(14) Cui, Y.; Yue, Y.; Qian, G.; Chen, B. Luminescent Functional Metal−Organic Frameworks. *Chem. Rev.* **2012**, *112*, 1126−1162.

(15) Wang, Z.; Li, X. Y.; Liu, L. W.; Yu, S. Q.; Feng, Z. Y.; Tung, C. H.; Sun, D. Beyond Clusters: Supramolecular Networks Self Assembled from Nanosized Silver Clusters and Inorganic Anions. *Chem. - Eur. J.* **2016**, *22*, 6830−6836.

(16) Jia, W. W.; Zhang, J.; Fan, R. Q.; Zhu, K.; Gai, S.; Tao, T.; Ji, C. S.; Nai, H. M.; Yang, Y. L. A Pitaya-Inspired Modular Cylindrical MOF-Based Capsule Design for Pesticide Signal Probes. *ACS Appl. Mater. Interfaces* **2023**, *15*, 11163−11174.

(17) Jia, W. W.; Fan, R. Q.; Zhang, J.; Zhu, K.; Gai, S.; Yin, Y. Y.; Yang, Y. L. Smart MOF-on-MOF Hydrogel as a Simple Rod-shaped Core for Visual Detection and Effective Removal of Pesticides. *Small* **2022**, *18*, No. 2201510.

(18) Zhang, H. J.; Fan, R. Q.; Chen, W.; Fan, J. Z.; Dong, Y. W.; Song, Y.; Du, X.; Wang, P.; Yang, Y. L. 3D Lanthanide Metal−Organic Frameworks Based on Mono-, Tri-, and Heterometallic Tetranuclear Clusters as Highly Selective and Sensitive Luminescent Sensor for Fe^{3+} and Cu^{2+} Ions. *Cryst. Growth Des.* **2016**, *16*, 5429−5440.

(19) Li, W. C.; Liu, L. Y.; Li, X. T.; Ren, H.; Zhang, L.; Parvez, M. K.; Al-Dosari, M. S.; Fan, L. M.; Liu, J. Q. A Ni(II) MOF-Based Hypersensitive Dual-Function Luminescent Sensor towards the 3-Nitrotyrosine Biomarker and 6-Propyl-2-Thiouracil Antithyroid Drug in Urine. *J. Mater. Chem. B* **2024**, *12*, 11800.
(20) Liu, X.; Li, X. T.; Li, W. C.; Liu, L. L.; Ren, H.; Jing, H. X.; Zhang, L.; Yin, J. G.; Fan, L. M. Eu(III) Encapsulation Strategy to Construct Intelligent Ratiometric Luminescent Sensor for Efficient Detection of Phenylglyoxylic Acid Biomarker in Bodily Fluids. *Microchem. J.* **2024**, *207*, No. 112127.
(21) Wang, G. D.; Li, Y. Z.; Shi, W. J.; Zhang, B.; Hou, L.; Wang, Y. Y. A Robust Cluster-Based Eu-MOF as Multi-Functional Fluorescence Sensor for Detection of Antibiotics and Pesticides in Water. *Sens. Actuators, B* **2021**, *331*, No. 129377.
(22) Gutierrez-Serpa, A.; Pacheco-Fernandez, I.; Pasan, J.; Pino, V. Metal−Organic Frameworks as Key Materials for Solid-Phase Microextraction Devices. *Separations* **2019**, *6*, 47.
(23) Duo, H. X.; Yue, J. Y.; Wan, X. F.; Sha, L. C.; Hou, X. D.; Zhu, Q. Recent Advances in Synthesis and Applications of Metal−Organic Frameworks for Sample Preparation in Antibiotic Analysis. *Microchem. J.* **2023**, *193*, No. 109053.
(24) Song, Y.; Fan, R. Q.; Wang, X. M.; Gao, S.; Du, X.; Wang, P.; Yang, Y. L. Direct Observation of Fast Single-Crystal-to-Single-Crystal Transformation from Cu^{II}-Framework to Cu^{I}-Chain Mediated by Ascorbic Acid: a Large Emission Shift of Two Valence-Tautomeric Copper Coordination Polymers. *CrystEngComm* **2016**, *18*, 1878.
(25) Wang, X. M.; Fan, R. Q.; Qiang, L. S.; Wang, P.; Yang, Y. L.; Wang, Y. L. Crystal Transformation Synthesis of a Highly Stable Fluorescent 3D Indium-Tetranuclear $\{In_4(\mu_2\text{-}OH)_3\}$ Building Block Based Metal Organic Framework through a Dinuclear Complex. *Dalton Trans.* **2014**, *43*, 16152.
(26) Song, Y. M.; Luo, F.; Luo, M. B.; Liao, Z. W.; Sun, G. M.; Tian, X. Z.; Zhu, Y.; Yuan, Z. J.; Liu, S. J.; Xu, W. Y.; Feng, X. F. The Application of Single-Crystal-to-Single-Crystal Transformation towards Adjustable SMM Properties. *Chem. Commun.* **2012**, *48*, 1006.
(27) Xing, K.; Fan, R. Q.; Du, X.; Song, Y.; Chen, W.; Zhou, X. S.; Zheng, X. B.; Wang, P.; Yang, Y. L. A Windmill-Like Zn_3L_2 Cage Exhibiting Conformational Change Imparted Sensing for DMA and Highly Selective Naked-Eye Detection of Co^{2+} Ion by Dynamic Quenching. *Sens. Actuators, B* **2018**, *257*, 68−76.
(28) Gai, S.; Zhang, J.; Fan, R. Q.; Xing, K.; Chen, W.; Zhu, K.; Zheng, X. B.; Wang, P.; Fang, X. K.; Yang, Y. L. Highly Stable Zinc Based Metal-Organic Frameworks and Corresponding Flexible Composites for Removal and Detection of Antibiotics in Water. *ACS Appl. Mater. Interfaces* **2020**, *12*, 8650−8662.
(29) Gai, S.; Fan, R. Q.; Zhang, J.; Sun, J. K.; Li, P. X.; Geng, Z. Q.; Jiang, X.; Dong, Y. Y.; Wang, J. Q.; Yang, Y. L. Structural Design of Low Toxic Metal−Organic Frameworks for Multifunction Detection towards Organic and Inorganic Contaminants from Water. *Inorg. Chem.* **2021**, *60*, 10387−10397.
(30) Chi, W. M.; Yu, F.; Dong, G. H.; Zhang, W. Z.; Chai, D. F.; Han, Pd.; Zhao, M.; Li, J. L.; Zhang, X. H. A Novel Peony-Shaped ZnO/Biochar Nanocomposites with Dominant {100} Facets for Efficient Adsorption and Photocatalytic Removal of Refractory Contaminants. *Colloids Surf., A* **2024**, *695*, No. 134291.
(31) Chen, J.; Zhang, M.; Zhang, S.; Cao, K.; Mao, X.; Zhang, M.; He, L.; Dong, X.; Shu, J.; Dong, H.; Zhai, F.; Shen, R.; Yuan, M.; Zhao, X.; Wu, G.; Chai, Z.; Wang, S. Metal−Organic Framework @ Metal Oxide Heterostructures Induced by Electron-Beam Radiation. *Angew. Chem., Int. Ed.* **2022**, *134*, No. e202212532.
(32) Jia, W. W.; Fan, R. Q.; Zhang, J.; Zhu, K.; Gai, S.; Nai, H. M.; Guo, H. Q.; Wu, J. K.; Yang, Y. L. Home-Made Multifunctional Auxiliary Device for In-Situ Imaging Detection and Removal of Quinclorac Residues through MOF Decorated Gel Refills. *Chem. Eng. J.* **2022**, *450*, No. 138303.
(33) Mukhopadhyay, A.; Jindal, S.; Savitha, G. J.; Moorthy, N. Temperature-Dependent Emission and Turn-Off Fluorescence Sensing of Hazardous ″Quat″ Herbicides in Water by a Zn-MOF Based on a Semi-Rigid Dibenzochrysene Tetraacetic Acid Linker. *Inorg. Chem.* **2020**, *59*, 6202.
(34) Xing, K.; Fan, R.; Gao, S.; Wang, X.; Du, X.; Wang, P.; Fang, R.; Yang, Y. Controllable Synthesis of Zn/Cd(II) Coordination Polymers: Dualemissive Luminescent Properties, and Tailoring Emission Tendency under Varying Excitation Energies. *Dalton Trans.* **2016**, *45*, 4863−4878.
(35) Wang, A. N.; Fan, R. Q.; Pi, X. X.; Hao, S. E.; Zheng, X. B.; Yang, Y. L. N-Doped Porous Carbon Derived by Direct Carbonization of Metal−Organic Complexes Crystal Materials for SO_2 Adsorption. *Cryst. Growth Des.* **2019**, *19*, 1973−1984.
(36) Wang, A. N.; Fan, R. Q.; Dong, Y. W.; Chen, W.; Song, Y.; Wang, P.; Hao, S. E.; Liu, Z. W.; Yang, Y. L. (E)-4-Methyl-N-((Quinolin-2-Yl)Ethylidene)Aniline as Ligand for IIB Supramolecular Complexes: Synthesis, Structure, Aggregation-Induced Emission Enhancement and Application in PMMA-Doped Hybrid Material. *Dalton Trans.* **2017**, *46*, 71−85.
(37) Janczak, J.; Prochowicz, D.; Lewinski, J.; Fairen-Jimenez, D.; Bereta, T.; Lisowski, J. Trinuclear Cage-Like ZnII Macrocyclic Complexes: Enantiomeric Recognition and Gas Adsorption Properties. *Chem. - Eur. J.* **2016**, *22*, 598−609.
(38) Yang, Y.; Ren, G.; Yang, W.; Qin, X.; Gu, D.; Liang, Z.; Guo, D. Y.; Qinhe, P. A New MOF-Based Fluorescent Sensor for the Detection of Nitrofuran Antibiotics. *Polyhedron* **2021**, *194*, 114923−114929.
(39) Senthilkumar, S.; Goswami, R.; Smith, V. J.; Bajaj, H. C.; Neogi, S. Pore Wall-Functionalized Luminescent Cd(II) Framework for Selective CO_2 Adsorption, Highly Specific 2,4,6-Trinitrophenol Detection, and Colorimetric Sensing of Cu^{2+} Ions. *ACS Sustainable Chem. Eng.* **2018**, *6*, 10295−10306.
(40) Gao, S.; Fan, R. Q.; Wang, X. M.; Qiang, L. S.; Wei, L. S.; Wang, P.; Zhang, H. J.; Yang, Y. L.; Wang, Y. L. An Insight into the Controllable Synthesis of Cd(II) Complexes with a New Multifunctional Ligand and its Application in Dye-Sensitized Solar Cells and Luminescence Properties. *J. Mater. Chem. A* **2015**, *3*, 6053−6063.
(41) Tard, C. D.; Perruchas, S.; Maron, S. B.; Goff, X. F.; Le, F.; Guillen, O.; Garcia, A.; Vigneron, J.; Etcheberry, A.; Gacoin, T.; Boilot, J. P. Thermochromic Luminescence of Sol-Gel Films Based on Copper Iodide Clusters. *Chem. Mater.* **2008**, *20*, 7010−7016.
(42) Benito, Q.; Goff, X. F.; Nocton, G.; Fargues, A.; Garcia, A.; Berhault, A.; Kahlal, S. J.; Saillard, Y.; Martineau, C.; Trebosc, J.; Gacoin, T.; Boilot, J. P.; Perruchas, S. Geometry Flexibility of Copper Iodide Clusters: Variability in Luminescence Thermochromism. *Inorg. Chem.* **2015**, *54*, 4483−4494.
(43) Wei, W.; Lu, R.; Tang, S.; Liu, X. Highly Cross-Linked Fluorescent Poly(Cyclotriphosphazene-Co-Curcumin) Microspheres for the Selective Detection of Picric Acid in Solution Phase. *J. Mater. Chem. A* **2015**, *3*, 4604−4611.
(44) Wang, X. S.; Li, L.; Yuan, D. Q.; Huang, Y. B.; Cao, R. Fast Highly Selective and Sensitive Anionic Metal−Organic Framework with Nitrogen-Rich Sites Fluorescent Chemosensor for Nitro Explosives Detection. *J. Hazard. Mater.* **2018**, *344*, 283−290.
(45) Wan, G. H.; Cui, H.; Zheng, H. S.; Zhou, H.; Liu, L. J.; Yu, X. F. Determination of Tetracyclines Residues in Honey Using High-Performance Liquid Chromatography with Potassium Permanganate-Sodium Sulfite-Beta-Cyclodextrin Chemiluminescence Detection. *J. Chromatogr. B* **2005**, *824*, 57−64.
(46) Zhan, X.; Hu, G.; Wagberg, T.; Zhan, S.; Xu, H.; Zhou, P. Electrochemical Aptasensor for Tetracycline Using a Screen-Printed Carbon Electrode Modified with an Alginate Film Containing Reduced Graphene Oxide and Magnetite (Fe_3O_4) Nanoparticles. *Microchim. Acta* **2016**, *183*, 723−729.
(47) Liu, B.; Zhang, B.; Chen, G.; Tang, D. Biotin-Avidin-Conjugated Metal Sulfide Nanoclusters for Simultaneous Electrochemical Immunoassay of Tetracycline and Chloramphenicol. *Microchim. Acta* **2014**, *181*, 257−262.
(48) Rodriguez, J. A.; Espinosa, J.; Aguilar-Arteaga, K.; Ibarra, I. S.; Miranda, J. M. Determination of Tetracyclines in Milk Samples by

https://doi.org/10.1021/acsomega.4c10594
ACS Omega 2025, 10, 3165−3175

Magnetic Solid Phase Extraction Flow Injection Analysis. *Microchim. Acta* **2010**, *171*, 407−413.
(49) Nagel, O. G.; Molina, M. P.; Althaus, R. L. Optimization of Bioassay for Tetracycline Detection in Milk by Means of Chemometric Techniques. *Lett. Appl. Microbiol.* **2011**, *52*, 245−252.
(50) Chen, X.; Zhao, L.; Tian, X.; Lian, S.; Huang, Z.; Chen, X. A Novel Electrochemiluminescence Tetracyclines Sensor Based on a $Ru(Bpy)_3^{2+}$-Doped Silica Nanoparticles/Nafion Film Modified Electrode. *Talanta* **2014**, *129*, 26−31.
(51) Wang, P.; Wu, T. H.; Zhang, Y. Novel Silver Nanoparticle-Enhanced Fluorometric Determination of Trace Tetracyclines in Aqueous Solutions. *Talanta* **2016**, *146*, 175−180.
(52) Yang, Y.; Niu, H.; Zhang, H. Direct and Highly Selective Drug Optosensing in Real, Undiluted Biological Samples with Quantum-Dot-Labeled Hydrophilic Molecularly Imprinted Polymer Microparticles. *ACS Appl. Mater. Interfaces* **2016**, *8*, 15741−15749.
(53) Wen, L.; Zheng, X.; Lv, K.; Wang, C.; Xu, X. Two Aminodecorated Metal−Organic Frameworks for Highly Selective and Quantitatively Sensing of Hg^{II} and Cr^{VI} in Aqueous Solution. *Inorg. Chem.* **2015**, *54*, 7133−7135.
(54) Malik, A. H.; Iyer, P. K. Conjugated Polyelectrolyte Based Sensitive Detection and Removal of Antibiotics Tetracycline from Water. *ACS Appl. Mater. Interfaces* **2017**, *9*, 4433−4439.
(55) Shi, Z. Q.; Guo, Z. J.; Zheng, H. G. Two Luminescent Zn(II) Metal−Organic Frameworks for Exceptionally Selective Detection of Picric Acid Explosives. *Chem. Commun.* **2015**, *51*, 8300−8303.
(56) Nagarkar, S. S.; Desai, A. V.; Ghosh, S. K. A Fluorescent Metal−Organic Framework for Highly Selective Detection of Nitro Explosives in the Aqueous Phase. *Chem. Commun.* **2014**, *50*, 8915−8918.
(57) Pramanik, S.; Zheng, C.; Zhang, X.; Emge, T. J.; Li, J. New Microporous Metal−Organic Framework Demonstrating Unique Selectivity for Detection of High Explosives and Aromatic Compounds. *J. Am. Chem. Soc.* **2011**, *133*, 4153−4155.

https://doi.org/10.1021/acsomega.4c10594
ACS Omega 2025, 10, 3165−3175